Fotogrametría para la caracterización de rugosidad superficial en aplicaciones SAR

Mieza, M. Soledad [1] Kovac, Federico D. [1]

1 Facultad de Ingeniería, UNLPam, (6360) General Pico-La Pampa, Argentina
smieza@ing.unlpam.edu.ar, kovacf@ing.unlpam.edu.ar

Resumen. En zonas agrícolas, las variables asociadas al suelo que más contribuyen al coeficiente de retrodispersión SAR son la rugosidad y la humedad volumétrica. Dado que desacoplar los efectos de ambas suele ser complejo, en este trabajo proponemos una metodología para caracterizar la rugosidad de suelo, en particular para aplicaciones SAR, en zonas agrícolas. Los métodos tradicionales, como la utilización de perfilómetros o tablas graduadas suelen ser poco prácticos, muy laboriosos y limitados a mediciones unidimensionales. Existen otras tecnologías, como los láseres, pero son inaccesibles a los fines prácticos por razones económicas y técnicas. En este trabajo proponemos una metodología basada en técnicas fotogramétricas avanzadas utilizando mayoritariamente paquetes de software educativos. Evaluamos la metodología propuesta sobre dos zonas piloto representativas (de aproximadamente 1 m^2); una con un patrón superficial aleatorio y otra donde simulamos surcos a distancias de laboreo agrícola típicas (52 cm.). Como resultado se obtuvieron modelos digitales de las superficies de alta resolución, que permitieron estimar los valores de las variables usualmente utilizadas en el entorno SAR para caracterizar la rugosidad superficial como son el desvío standard de la altura o altura rms y la longitud de correlación. Además, se diseñó una metodología para obtener, a partir de los modelos digitales de superficie, medidas de rugosidad multiescala a través del análisis de Fourier. Los promisorios resultados de esta metodología simple y de bajo costo, estimamos, permitirá obtener información precisa de la rugosidad de suelo para el desarrollo de aplicaciones SAR en el contexto de las misiones Argentinas SAOCOM.

Palabra clave: Rugosidad de suelo, SAR, fotogrametría, rugosidad multiescala

Received May 2024; Accepted June 2024; Published July 2024
https://doi.org/10.24215/15146774e051

ISSN 1514-6774

Soil roughness characterization by photogrammetric techniques

Towards SAR modeling

Mieza, M. Soledad [1] Kovac, Federico D. [1]

1 Facultad de Ingeniería, UNLPam, (6360) General Pico-La Pampa, Argentina
smieza@ing.unlpam.edu.ar, kovacf@ing.unlpam.edu.ar

Abstract. Soil roughness and volumetric moisture are the two main soil-related variables influencing the SAR backscattering coefficient. Since it is usually challenging to decouple the effect of each, in this work, we propose a methodology to estimate soil roughness, mainly in agricultural environments. The traditional methods, using graduated tables and profilometers, are laborious and spatially limited. The use of lasers is feasible, but they are normally inaccessible. This work proposes a methodology based on photogrammetric techniques using primarily educational software. We tested the method over two bare soil 1m-areas, one with a random surface pattern and another where we simulated typical crop rows (52 cm apart). As a result, highly accurate surface three-dimensional digital models were obtained. We then extracted the standard deviation of the surface height and the correlation length, the main roughness parameters required in SAR modeling. Additionally, we were able to extract other relevant information, such as the predominant spatial structure directions and height profiles from the autocorrelation function and the multiscale roughness through Fourier analysis. Given the excellent results of this fast and low-cost methodology, we estimate it could provide precise and systematic information on soil roughness for operational applications in the SAR context in view of Argentina's SAOCOM missions.

Keywords: Soil roughness, SAR, photogrammetry, multiscale roughness.

1 Introduction

Estimating surface roughness for extensive agriculture applications can be complex due to the varying sizes and spatial variability of agricultural plots. Some traditional methods available to accomplish this task include graduated tables or a profilometer. However, these methods are invasive and can be time-consuming, localized, and limited to one dimension. On the other hand, non-contact techniques like lasers and acoustic signals are costly and not easily accessible. Remote sensing data can also be utilized, but it requires extensive calibration and depends on the image's characteristics and scale. Photogrammetry-based techniques have emerged as a promising methodology for laboratory or field studies, assuming a certain level of proficiency in this method [1].

SAR data portrays a physical magnitude, the backscatter coefficient (σ^0). In agricultural areas, this coefficient can be influenced by factors such as soil conditions and the characteristics of vegetation cover. Surface roughness and volumetric moisture significantly affect soil backscattering. These variables are often intertwined, making it difficult to distinguish their individual effects. As pointed out by [2], another aspect to consider is that natural surface roughness consists of continuous roughness scales. Since most SAR sensors' operational wavelengths (λ) usually range from a few centimeters to tens of centimeters, a centimeter-scale roughness measurement is commonly used for SAR scattering modeling. However, a better understanding of the surface scattering process could be achieved if several scale roughness could be obtained. For example, [3] proposed a dual-scale surface roughness that they could relate to seedbed rows and wheel tracks of the machinery used. Also, the issue of the influence of the spatial sampling interval in the microwave response of agricultural surfaces is addressed by [4].

Argentina has developed the SAOCOM missions, which include two L-band Synthetic Aperture Radars (SARs) that operate at a wavelength (λ) of 23.5 cm. Since Argentina's economy heavily relies on agricultural products grown over vast areas of land, these missions primarily focus on applications related to agriculture [5]. The two SARs form a constellation with four COSMO-SkyMed (CSK) Italian Space Agency satellites operating at the X Band (λ= 3.1 cm). This setup enables data to be gathered at varying frequencies close in time over the same study area. Combining SAR data at different bands presents a unique opportunity to gain insights into the complex interplay between agricultural variables since the interaction between the incoming waves and the earth's surface elements is wavelength-dependent.

Thus, this study aimed to assess a technique for surface roughness characterization on typical agricultural soils based on digital surface models (DSMs) derived from photogrammetric methods. The main objective was to develop a reliable, accurate, user-friendly, and cost-effective method.

2 Methodology

2.1 DSM generation and evaluation

To carry out the methodology, we selected two pilot areas, each measuring approximately one square meter (1 x 1.02 meters). In the first plot, the soil was left undisturbed, while in the second plot, we replicated the conventional rows typically used for summer crops in central Argentina, such as soybeans, maize, and sunflower. The rows were positioned at a distance of 52 cm from one another and had an average height of 10 cm, as illustrated in Figure 1.

Fig. 1. Study areas (approximately 1m^2 each). The undisturbed soil is on the left image, and the simulated crop rows are on the right.

We utilized a frame with known dimensions and added external elements, also known as phantoms, to facilitate the alignment of images and scale the models obtained. In the course of the experiment, we made use of phantoms consisting of wooden rods with established dimensions. We captured about 100 images for each surface using a 12 MPx compact digital camera, employing methods similar to those previously tested on various artificial surfaces [6]. The approach involved taking photos from different angles at varying heights up to 1.20 m approximately and also a set following a regular ideal grid pattern with the camera positioned perpendicular to the ground. It's worth noting that no GPS or geolocation data is needed to be collected for the camera positions. A schematic diagram of the ideal camera positions is in Fig. 2 (a), and in Fig. 2 (b), actual camera locations for one of the study areas.

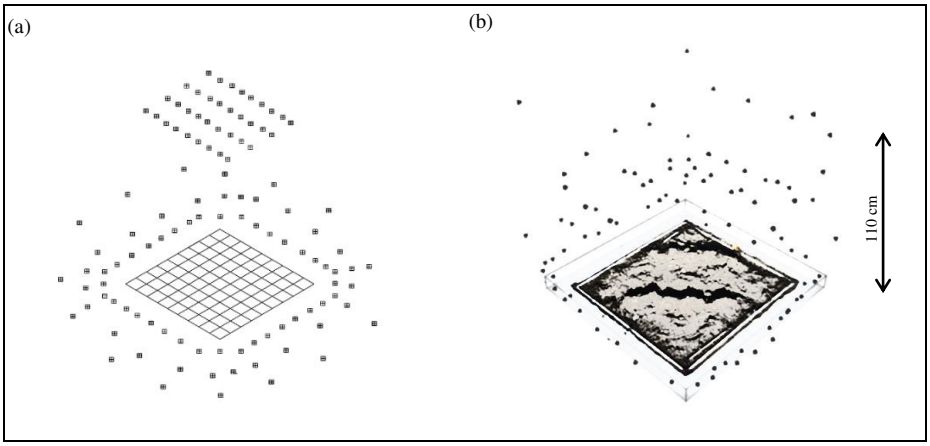

Fig. 2. (a) Ideal acquisition setting and (b) Actual acquisition pattern

The digital surface models were created using advanced photogrammetric techniques that rely on *structure from motion* [7]. Different fields of study utilize this method [8].

Specifically, previous studies such as those by [9] and [10] have applied it to analyze surface roughness. In contrast to conventional photogrammetry techniques, this method greatly simplifies reconstructing a 3D surface due to the automatic acquisition of the camera's position and orientation throughout the process, enabling greater flexibility in acquisition patterns without requiring the measurement of the camera's position and angle for every shot.

We used Autodesk©'s RecapPhoto© software's cloud-based educational version to generate the DSMs. Fig. 3 showcases several photos captured of the simulated crop rows area. One photo offers a partial view near ground level, another features a diagonal view at a medium height, and the third presents a full view with the camera facing downward. These pictures were utilized in their original form without additional trimming or conditioning. One of the software's interesting capabilities is its insensitivity to external objects (like the trees seen in the first photo) or shadows produced during the data collection. The software automatically selects the best images for the final reconstruction from those uploaded by the operator.

Fig. 3. Sample photographs

After completing the online processing, we downloaded the DSMs to the local interface. We then clipped, aligned, and scaled the models. Lastly, we exported the clouds of points (x,y,z) in tabular form and generated raster images for further analysis.

To ensure consistency, a second DSM of the random surface was created using the same set of photographs and compared to the first model because a-priori, the method does not ensure repeatability when applied to the same data set.

We analyzed the relative error (ε) using Equation (1) to assess accuracy. It was calculated using established dimensions as references, such as phantom sizes and frame measurements.

$$\varepsilon(\%) = \frac{|d_{mod} - d_{real}|}{d_{real}} \times 100 \qquad (1)$$

Where d_{mod} and d_{real} are the measurements performed on the models and the actual surfaces respectively.

2.2 Surface roughness parameters estimation

In SAR applications, surface roughness is typically described by two statistical parameters: the standard deviation (**s**) of the surface height from a reference height or rms height and the correlation length (ℓ), which indicates the surface's periodicity [2]. The latter is defined as the distance at which the normalized autocorrelation function (ACF) decays to 1/e [11] and is an estimate of the statistical independence between two points on the surface; if they are separated by a distance greater than l/e, then they can be considered statistically independent. In the limiting case of a specular surface, ℓ tends to infinity.

The calculation of the standard deviation of the surface height is a straightforward process based on the DSM height values. Regarding the autocorrelation length, the approach involves segmenting the two-dimensional ACF [12]. The ACF is an image with the same size as the original, and each pixel value is related to the degree of correlation between the original image and a displaced version in all directions. The ACF reaches its maximum value at the center of the image, where there is no displacement. When the image contains isotropic structures, the ACF shows a similar decay rate in all directions. However, when the picture exhibits anisotropic patterns, the decay rate may differ, resulting in elongated contour lines in the direction of the greatest correlation. Based on the method used in [13], we established the cut-off point for determining the correlation length at 0.4 (~1/e) of the maximum value of the normalized ACF. We used ellipses to approximate the isolines in this scenario, as they do not typically correspond with known geometric shapes. The minor and major semi-axes of the ellipses were then used to estimate the minimum and maximum autocorrelation lengths, respectively.

It is also essential to determine the orientation of surface patterns (e.g., crop rows) because, based on the SAR incident angle, interference patterns (such as Bragg scattering) may appear in the images. The 2D ACF of the DSM can also be employed to estimate the average size and orientation of spatial structures. This technique has been applied at various scales, like determining the size of grains in materials [14] or estimating the average size and shape of topographic structures [15].

2.3 Multiscale roughness

Fourier analysis was used to extract multiscale roughness measurements, a technique widely used in signal processing and electronics for signal filtering [16]. In a Fourier-transformed image, its entries depict the spatial frequency components of the original image, both horizontally and vertically. Spatial frequency is akin to time-frequency for a signal; a high-frequency sinusoidal function oscillates rapidly, while a low-frequency function changes gradually with time. Similarly, an image with high spatial frequency displays frequent changes in brightness. A typical image comprises vertical and horizontal components of varying strengths, each with different spatial frequencies. These components are precisely what the discrete Fourier transform characterizes. In the present study, we have straightforwardly estimated different roughness scales through the frequency domain analysis.

The raster format DSMs were converted into the frequency domain using the Fast Fourier Transform (FFT). We used [18] for the Fourier analysis, and the post-processing and analysis were performed in [17]. This conversion process transforms the image into a series of two-dimensional sine waves of different frequencies. A complex number represents each resulting pixel once an image is transformed into its frequency domain. For visualization purposes, the magnitude of each complex number is calculated, and the dynamic range is adjusted accordingly. The FFT magnitude image is represented in a new coordinate space (u,v) related to the frequencies. The sampling increment in the frequency domain (Δu, Δv) is related to the pixel size in the spatial domain and also to the size of the original image as follows:

$$(\Delta u, \Delta v)=\left(\frac{1}{M\Delta x}, \frac{1}{N\Delta y}\right) \qquad (2)$$

Where
M = horizontal size in pixels of the original image.
N = vertical size in pixels of the original image.
Δx, Δy = pixel size in the spatial domain in the x and y directions.

The new image is symmetric about its origin (u, v) = (0, 0), located at the center of the image. Then, lower frequencies are plotted near the origin, while higher frequencies are plotted further out.

Once in the frequency domain, the spectrum was subdivided into three subsets employing low and high pass filters. In the Fourier domain, the filtering process is straightforward and usually faster than applying convolution filters in the spatial domain. For the low-pass operation, for example, once the cut-off frequency (D_0) is selected, the filtering process only leaves those frequencies that comply with $u^2+v^2 < D_0^2$; that is, those pixels within a circle of radius D_0 in the (u,v) space [18]. Similarly, the high-pass filtering was performed. The criteria for the selection of D_0, in this case, was based on the spectrum statistics.

It should be mentioned that the number of intervals and cut-off frequencies can be arbitrarily selected to fulfill different objectives for any given application.

Each frequency domain subset was then converted back into the spatial domain through the Inverse FFT (IFFT).

Finally, three raster images of the surfaces were obtained: one showing the large-scale undulation of the surface (low frequencies), another for the medium-scale roughness, and the last one associated with the high-spatial frequency variations of the surface height.

3 Results

3.1 DSM

The resulting DSMs that have been scaled and cropped to remove any interference from the borders and phantoms are shown in Fig. 4. They are presented in both rendered and raster versions. Short videos of both models can be found in [19] for the random surface, and for the simulated crop rows model, please go to [20]. In both cases, increasing the visualization resolution on YouTube is recommended for better results.

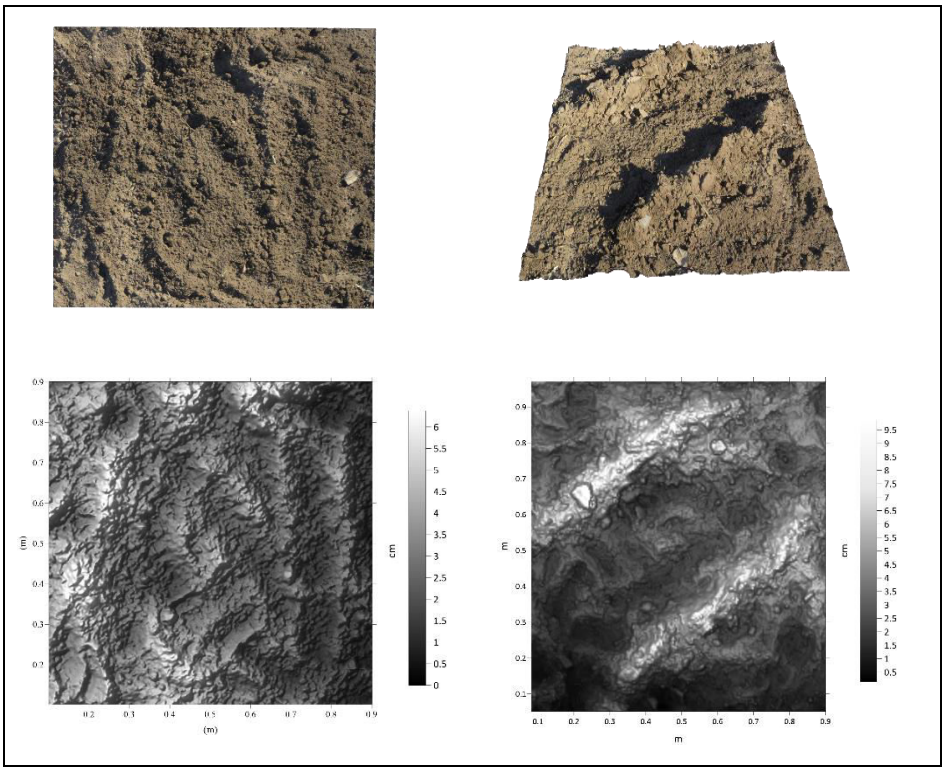

Fig. 4. Resulting DSMs, on the left, the one corresponding to the random surface, and on the right, the surface simulating crop rows.

After conducting the accuracy assessment for 10 measurements on each DSM, it was found that the relative error in all cases was less than 2%, consistent with previous results obtained using a similar methodology for artificial surfaces [21]. Furthermore, upon analysis of a second DSM generated from the same data set (for the random surface), it was found that the method was robust, with differences between the two DSMs being less than 2.5%.

3.2 Surface roughness parameters estimates

The data was post-processed and resulted in raster images shown in Fig. 5 and Fig. 6. Each pixel in the raster images corresponds to the digital model height value. A transect was also traced in both figures, and the associated height profiles are depicted below the raster images.

The rms height values were 0.9 cm for the first surface and 1.7 cm for the second.

Also, the corresponding ACF functions are shown. The central area indicates where the maximum ACF is observed and corresponds to a null displacement of the raster image. The 0.4 contour lines are also presented, which indicates the typical size of the structures in the terrain.

For the random surface (Fig.5), the image shows a slight deformation in the vertical direction associated with the semi-major axis of the ellipse. However, it is essential to mention that the origin of the coordinate system was arbitrarily established in one of the corners of the frame used to delimit the area of interest, so it does not make physical sense.

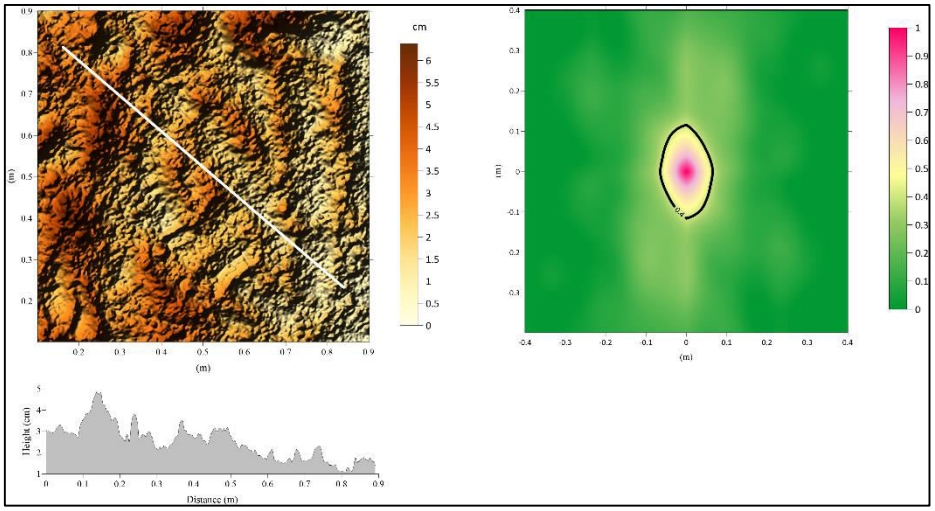

Fig. 5. Raster image of the random soil sample and corresponding ACF.

By approximating the isoline with an ellipse, the values corresponding to the major and minor semi-axes were extracted from the graph, resulting in 11.4 cm and 6.7 cm, respectively. These values are indicative of the maximum and minimum correlation lengths.

For the other surface (Fig. 6), the minimum and maximum ℓ were 7 cm and 23 cm, respectively. The orientation with respect to the horizontal was estimated at approximately 37.5°. In the image of the ACF, the impact of the spatial pattern of rows can be observed as it leads to an increase in the autocorrelation values in the labeled areas A and B.

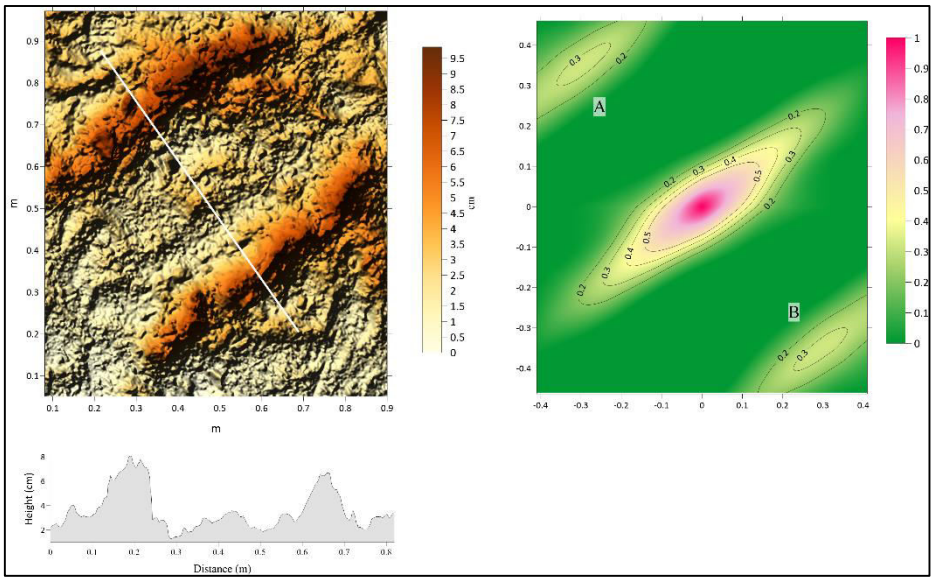

Fig. 6. Raster image of the simulated crop rows surface and corresponding ACF.

3.3 Multiscale roughness

The proposed methodology for extracting multiscale roughness was implemented for the soil sample with the simulated crop rows, as shown in Fig.7(a). Firstly, the FFT was applied, and its magnitude was calculated, as shown in Fig. 7 (b). The FFT magnitude and its corresponding histogram reveal varying frequencies within the image. The lower frequency could be related to coarser roughness scales, while the high frequencies are related to finer scales.

Moreover, the transformed image brings attention to two main directions in the Fourier image: one runs vertically and the other horizontally through the center. These directions stem from regular patterns in the original image's background that may not be evident in the spatial domain.

Then, in the frequency domain, the filtering process was applied based on these criteria: values below the mean (μ) minus one standard deviation (SD) ($D_0 < \mu - 1SD$) were filtered for low frequencies. Values ranging from the mean minus one standard deviation to the mean plus one standard deviation ($\mu - 1SD \leq D_0 \leq \mu + 1SD$) were retained for medium frequencies. The associated histogram and statistical parameters are shown below the FFT magnitude image. High frequencies were identified as values above the mean plus one standard deviation ($D_0 > \mu + 1SD$) and were filtered accordingly. Fig. 7 (c) shows the resulting FFT magnitude image after applying the low-frequency filter.

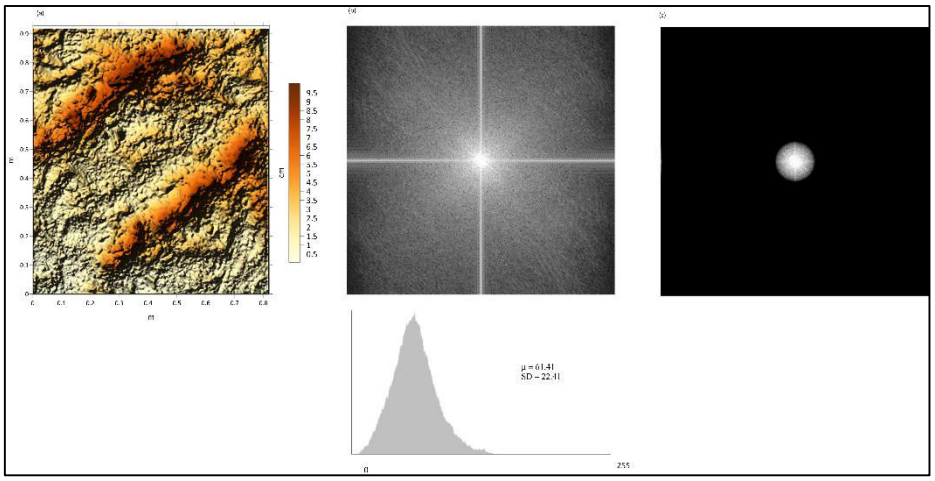

Fig. 7. (a) Raster image of the DSM with crop rows, (b) FFT magnitude of the image in (a) and associated histogram, and in (c) FFT magnitude after low-frequency filter was applied.

After applying the three filters, the IFFT converted each filtered FFT magnitude image back to the spatial domain. Figure 8 (a) represents the original DSM, while (b), (c), and (d) represent the filtered images back in the spatial domain for low, medium, and high-frequency spectrums, respectively. Additionally, the height profiles for the white transect at equivalent locations are presented for all images. The original profile can be considered a combination of the three profiles exhibiting different roughness scales.

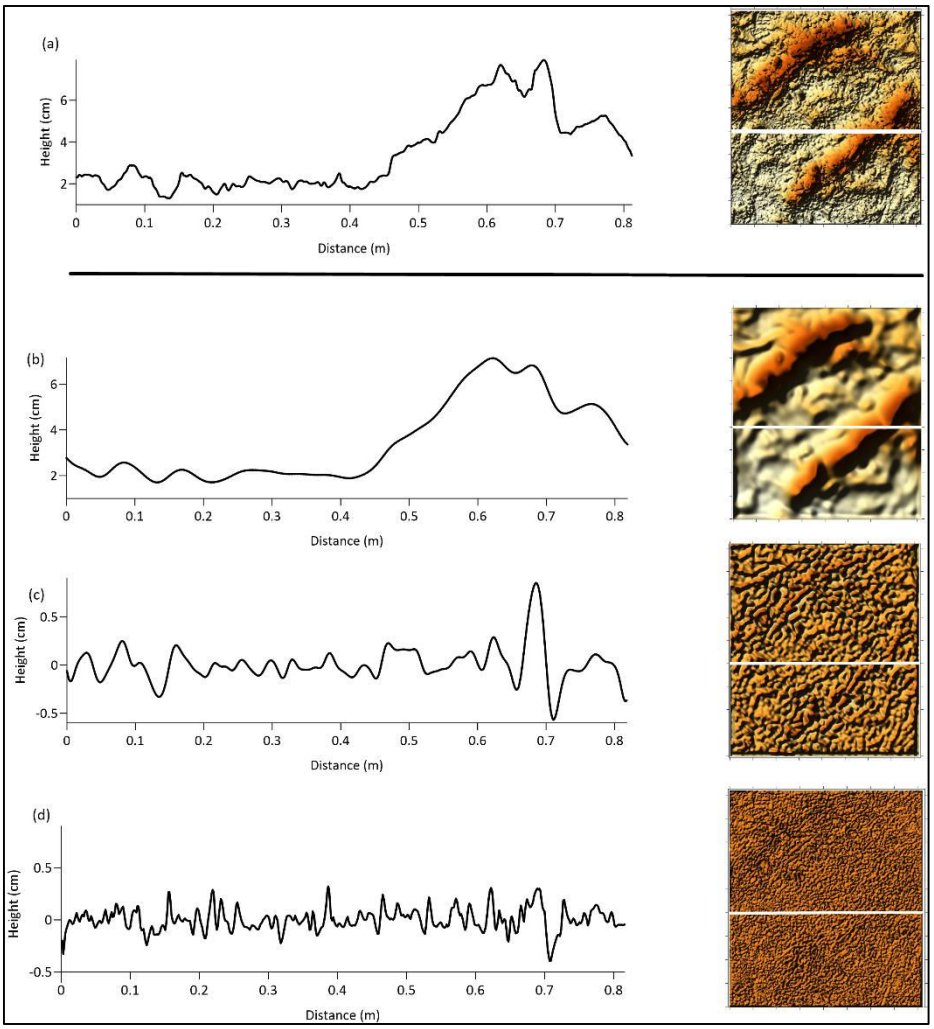

Fig. 8. (a) Height profile for the transect line in the original DSM with crop rows. (b),(c) and (d) Height profiles for the low, medium and high frequency roughness components.

4 Discussion

This study is part of a larger project that focuses on modeling the backscattering coefficient of crops in central Argentina. The study area is located in NE La Pampa, where no-till practices are primarily used for crop cultivation, resulting in soil roughness patterns within the range of the pilot studies presented in this work. Increasingly, farms are adopting precision agriculture techniques. While the degree of adoption varies

among producers, it is typical to identify three management zones within each plot where variable seed and fertilizer rates are applied.

Analyzing different scenarios through modeling is essential in utilizing SAR data effectively since several factors, including vegetation canopy geometry and moisture, area coverage, leaf area index, soil roughness, and moisture, influence the backscattering coefficient. Our ultimate goal is to create practical applications that can be utilized in the future, especially at the plot level.

The main objective of the work presented here was to measure the soil roughness, which was proven to be a challenging variable using the available methods, especially the autocorrelation length.

Understanding and modeling the effect of the soil in SAR backscatter is essential at the L Band (SAOCOM sensors) since, given the relatively large wavelengths, even with well-developed crops, radiation can penetrate the canopy and interact with the soil.

The results pleasantly surprised us, as they exceeded our expectations regarding accuracy, robustness, and simplicity.

When discussing the estimation of surface roughness, the possibility of using data obtained by Unmanned Aerial Vehicles (UAVs) may come up. While we did not conduct the experiments ourselves, it is important to note some limitations when collecting data with UAVs for roughness scales of this nature. Our experience with various surfaces indicates that images taken close to the ground are crucial to ensure the accuracy of the reconstruction. However, the effectiveness of UAVs at these low heights, which are generally only a few centimeters, can be questioned.

Undoubtedly, field measurements, particularly in remote sensing applications, pose certain challenges. Still, one of the main advantages is that only the photographs need to be taken in the fields, allowing multiple samples to be collected quickly by one or more teams.

Unfortunately, our experiment did not allow for the collection of more precise data, such as laser scanning, to compare the final roughness estimates, and the profilometer was deemed unsuitable due to its one-dimensional nature, its potential to alter the actual height during the measuring process, and its coarser resolution. However, we plan to compare this method with a 3D reconstruction of the surfaces using a newly acquired Artec3D scanner. This scanner boasts a nominal 3D resolution of up to 0.2 mm [22].

Roughness is not an absolute concept. In particular, a surface can be considered smooth or rough in SAR applications depending on the incoming wavelengths. The Fraunhofer roughness criterion that relates the rms height with the SAR wavelength (λ) and the incidence angle (θ) is usually used to quantify this. A surface, then, can be considered smooth if it complies with equation 3:

$$s < \frac{\lambda}{32 \cos \theta} \qquad (3)$$

Then, not all roughness scales are essential for all SAR images [2]. If we were to analyze the surfaces with SAR images, the various roughness scales, such as those in Fig. 8, would contribute differently to the backscattering coefficient. For example, Fig. 8

(b) represents the original surface's coarse roughness patterns. This new surface can also be characterized by its rms height and autocorrelation lengths that we denominated (s_b, ℓ_b). Then, the surface would appear flat for wavelengths longer than s_b and ℓ_b since no incoherent scattering occurs. As the wavelength is shortened so that it approaches the dimensions of s_b or ℓ_b, incoherent scattering appears, but the shorter scales Fig. 8 (c) and (d) do not play a significant role. Subsequently, the higher spatial frequencies contribute to the scattering process as the SAR wavelength is further reduced.

Finally, in the realm of Synthetic Aperture Radar (SAR) modeling, it is common practice to rely on a limited set of values for the root mean square (rms) height and correlation length parameters. The DSM's spatial dimensionality provides new opportunities to integrate more information into physical models.

5 Conclusions

In this paper, we demonstrate how photogrammetric techniques can be used to create 3D models of two usual surfaces found in agricultural settings to estimate surface roughness in the context of SAR applications. One surface has a random pattern, while the other simulates crop rows.

The digital models obtained are photo-realistic; if compared with photographs, in many cases, they are indistinguishable. The quantitative evaluation was consistent with the qualitative one, with a relative error of less than 2%. The method proved to be robust, with consistent reconstruction results from the same set of photos.

The method employed enables the determination of the required surface roughness parameters for SAR, namely the rms height and correlation length.

The acquisition of multiscale roughness measurements from surface structures represents a challenging task that is not easily achievable with conventional methods. Through Fourier analysis, an efficient methodology is presented for disentangling various roughness components in surface structures, resulting in a highly accurate representation of surface topography.

To accurately model roughness over larger areas, we plan to conduct more field-level studies to evaluate the methodology under different roughness conditions and analyze variability within individual fields or regions.

The results are satisfactory, and the method's simplicity, robustness, and low cost make it highly applicable for characterizing surface roughness in various fields, including SAR and other knowledge areas.

References

[1] W. Jester and A. Klik, "Soil surface roughness measurement - Methods, applicability, and surface representation," *Catena*, vol. 64, no. 2–3, pp. 174–192, 2005.

[2] F. Ulaby and D. Long, "chapter10," in *Microwave Radar and Radiometric Remote Sensing*, The University of Michigan Press, 2014, pp. 420–458.

[3] P. Marzahn, M. Seidel, and R. Ludwig, "Decomposing Dual Scale Soil Surface Roughness for Microwave Remote Sensing Applications," *Remote Sens.*, vol. 4, no. 7, pp. 2016–2032, Jul. 2012.

[4] M. E. Barber, F. M. Grings, J. álvarez-Mozos, M. Piscitelli, P. A. Perna, and H. Karszenbaum, "Effects of spatial sampling interval on roughness parameters and microwave backscatter over agricultural soil surfaces," *Remote Sens.*, vol. 8, no. 6, 2016.

[5] CONAE, "Objetivos de la mision SAOCOM." [Online]. Available: https://www.argentina.gob.ar/ciencia/conae/misiones-espaciales/saocom/objetivos. [Accessed: 12-May-2023].

[6] W. H. Fruccio, F. D. Kovac, M. S. Mieza, and M. Giménez Bertola, "Featured paper.Digital photogrammetric techniques in engineering education. (Original version in Spanish: Técnicas de fotogrametría digital destimadas a la formación de ingenieros)," in *Universidad Tecnológica Nacional VII Congreso Argentino de Ingeniería Mecánica y II Congreso Argentino de Ingeniería Ferroviaria : VII CAIM-II CAIFE*, 2021, pp. 39–51.

[7] S. Ullman and S. Brenner, "The interpretation of structure from motion," *Proc. R. Soc. London. Ser. B. Biol. Sci.*, vol. 203, no. 1153, pp. 405–426, Jan. 1979.

[8] G. Sansoni, M. Trebeschi, and F. Docchio, "State-of-the-art and applications of 3D imaging sensors in industry, cultural heritage, medicine, and criminal investigation," *Sensors*, vol. 9, no. 1, pp. 568–601, Jan. 2009.

[9] P. Marzahn, D. Rieke-Zapp, and R. Ludwig, "Assessment of soil surface roughness statistics for microwave remote sensing applications using a simple photogrammetric acquisition system," *ISPRS J. Photogramm. Remote Sens.*, vol. 72, pp. 80–89, 2012.

[10] S. Gharechelou, R. Tateishi, and B. A. Johnson, "A simple method for the parameterization of surface roughness from microwave remote sensing," *Remote Sens.*, vol. 10, no. 11, Nov. 2018.

[11] J. C. Russ, *The Image Processing Handbook, Fourth Edition*. CRC Press, 2002.

[12] R. P. Heilbronner, "The autocorrelation function: an image processing tool for fabric analysis," *Tectonophysics*, vol. 212, no. 3–4, pp. 351–370, 1992.

[13] A. A. de Ronde, R. Heilbronner, H. Stünitz, and J. Tullis, "Spatial correlation of deformation and mineral reaction in experimentally deformed plagioclase-olivine aggregates," *Tectonophysics*, vol. 389, no. 1–2, pp. 93–109, Sep. 2004.

[14] R. Heilbronner, "Analysis of bulk fabrics and microstructure variations using tesselations of autocorrelation functions," *Comput. Geosci.*, vol. 28, no. 4, pp. 447–455, 2002.

[15] M. S. Mieza, W. R. Cravero, F. D. Kovac, and P. G. Bargiano, "Delineation of site-specific management units for operational applications using the topographic position index in La Pampa, Argentina," *Comput. Electron. Agric.*, vol. 127, pp. 158–167, 2016.

[16] D. Sundararajan, *Fourier Analysis—A Signal Processing Approach*. Springer Singapore, 2018.

[17] "QGIS 3.16.".

[18] ERDAS, "ERDAS Field Guide ™ - Tutorial," no. November, p. 810, 2009.

[19] M. S. Mieza and F. D. Kovac, "DSM random surface," 2024. [Online]. Available: https://youtu.be/M4nSJ5a1ZzA.

[20] M. S. Mieza and F. D. Kovac, "DSM Row crops / DSM surcos simulados," 2024.

[Online]. Available: https://youtu.be/PqzQoLnBy9E.

[21] F. D. Kovac, W. H. Fruccio, and M. S. Mieza, “Modelado 3D de Superficies Regulares Utilizando Software Educativo,” in *ANALES DE SAIV 2021 SIMPOSIO ARGENTINO DE IMAGENES Y VISION (JAIIO)*, 2021, pp. 11–15.

[22] Artec Leo - Specification Sheet, "Artec Leo." [Online]. Available: https://www.artec3d.com/es/portable-3d-scanners/artec-leo#tech-specs.